Fuzzy model based object delineation via energy minimization

Krzysztof Chris Ciesielski,[a,b] Jayaram K. Udupa,[b] Dewey Odhner,[b] and Liming Zhao[b]

[a]Department of Mathematics, West Virginia University, Morgantown, WV 26506-6310

[b]Dept. of Radiology, MIPG, Univ. of Pennsylvania, Blockley Hall – 4th Floor, 423 Guardian Dr., Philadelphia, PA 19104-6021

ABSTRACT

We study the problem of automatic delineation of an anatomic object in an image, where the object is solely identified by its anatomic prior. We form such priors in the form of fuzzy models to facilitate the segmentation of images acquired via different imaging modalities (like CT, MRI, or PET), in which the recorded image properties are usually different. Our main interest is in delineating different body organs in medical images for automatic anatomy recognition (AAR).

The AAR system we are developing consists of three main components: (C1) building body-wide groupwise fuzzy anatomic models; (C2) recognizing the body organs geographically and then delineating them by employing the models; (C3) generating quantitative descriptions. This paper focuses on (C2) and presents a unified approach for model-based segmentation within which several different strategies can be formulated, ranging from model-based hard/fuzzy thresholding to model-based graph cut, fuzzy connectedness, and random walker methods and algorithms. This is an important theoretical advance.

The presented experiments clearly prove, that a fully automatic segmentation system based on the fuzzy models can indeed provide the reliable segmentations. However, the presented experiments utilize only the simplest versions of the methodology presented in the theoretical part of the paper. The full experimental evaluation of the methodology is still a work in progress.

1. INTRODUCTION AND GENERAL SET-UP

1.1. Basic terminology

We identify an *image* $I = \langle C, f\rangle$ with its *intensity function* $f\colon C \to \mathbb{R}^\nu$, that is, a map from its *domain*—a subset C of the 3-dimensional Euclidean space $\mathbb{R}^3$—into $\mathbb{R}^\nu$. The value $f(c)$ of f at c represents the image intensity (for $\nu = 1$) and, more generally, a ν-dimensional vector of measured quantities at c. Our main interest is in *digital images*, that is, in the case when C is a finite subset of $\mathbb{Z}^3$, usually of the rectangular form $C_1 \times \cdots \times C_3$ with each $C_i = \{1, \ldots, m_i\}$; however, as we point out via examples, our general set-up includes also the "continuous" cases, in which C is an open region in $\mathbb{R}^3$.

For the purpose of this paper, a *prior* (of an object of interest) is used to encode a spatial variability of the object it describes. Mathematically, it will be represented as a mapping $\ell\colon C \to [0, 1]$, to which we will refer as *labeling*, such that the number $\ell(c)$ represents a degree of membership that $c \in C$ belongs to the desired object. We take a fuzzy modeling approach [8]. Other alternatives such as statistical modeling or atlases (see e.g. [10]) will fit well into the hybrid delineation strategy described here as well. We assume that a rough recognition of the object of interest has been achieved which means that the model is placed fairly "close" to the actual object in the given image I, implying that the model matches the object roughly in size, position, and orientation. In fuzzy modeling, multitudes of objects in a body region are considered so as to bring severe constraints on object placement in I for effective recognition [8]. The objects are arranged in a hierarchy as a tree and the recognition process proceeds following the hierarchy. As we will see below, the delineation methods presented simultaneously optimize (fine) recognition and delineation. The general set up allows the process to be used in different ways—optimizing delineation only from a given starting recognition result, or performing optimization for both simultaneously.

1.2. Motivation and some background

In the theoretical considerations, we concentrate on purely geometric priors, to facilitate segmentations of images acquired via different imaging modalities (like CT and MRI), as in each modality the recorded image properties (intensities, resolution, etc) are different. However, the general problem set-up is not restricted to such restrictive choice of a prior. (In particular, we use image intensity information in our experiments.) Notice also that the geometric priors should be considerably more reliable for 3D images, since in such case the object shape is independent of the plane of view.

Medical Imaging 2013: Image Processing, edited by Sebastien Ourselin, David R. Haynor,
Proc. of SPIE Vol. 8669, 86693H · © 2013 SPIE · CCC code: 1605-7422/13/$18
doi: 10.1117/12.2006623

Some of the oldest and best studied image segmentation methods are purely image-based (pI) and focus on delineating objects based entirely on the information about objects that can be harnessed from the given image. Although these methods have many advantages, they have also many shortcomings. The shortcoming that we like to stress here is that they always require some additional parameters (like seeds indicating the object(s) and, sometimes, background) and, in general, it is almost impossible to run such algorithms without displaying the segmented image and giving some recognition input by an operator. One of the most important goals of the prior-based segmentation algorithms should be to make a segmentation task fully automatic, that is, not requiring human to examine the image prior to invoking the algorithm to get reliable output.

The vast majority among the pI methods choose the returned delineated object among those which optimize some energy (or cost) function. Moreover, the energies that are optimized via these algorithms are more and more recognized as belonging to the very few groups of energy functionals, with such recognition facilitating our understanding of the differences and similarities among the pI algorithms. For the prior-based segmentation algorithms the theory did not reach, as yet, such stage. Thus, the general set-up we describe in this section will attempt to make a progress towards reaching this stage. In the next section, on the other hand, we will concentrate on more specific energy functionals and on the algorithms that can optimize them.

1.3. Methods

The energy E we use for the optimization will contain two main components: the image based energy ε_i and the prior-based energy ε_p. Each of these energy components, ε_i and ε_p, can be defined as any energy used in the pI algorithms and it associates to an image $I = \langle C, f\rangle$ and its segmentation $x\colon C \to [0,1]$ the energy value, either $\varepsilon_i(x,f)$ or $\varepsilon_p(x,f)$. Notice, that x here is a *fuzzy set*, that is, the value $x(c)$ represents the degree of membership (or probability) of c belonging to the object of interest. Such objects are used by several algorithms, e.g., Random Walk [4] or the algorithms discussed in [3] and [6]. However, we will be mainly interested in the hard segmentations $x\colon C \to \{0,1\}$, in which case $x^{-1}(1) = \{c \in C\colon x(c) = 1\}$ is the delineated object.

Now, let $\mathcal{G}$ be a group of transformations of $\mathbb{R}^3$ used to match prior ℓ to image I and, for a given prior ℓ on $C \subset \mathbb{R}^3$ let $\hat{\ell}\colon \mathbb{R}^3 \to [0,1]$ denote an extension of ℓ. It can be assumed that $\hat{\ell}$ is an interpolation of ℓ. Then, for $g \in \mathcal{G}$ and a segmentation x, we define the energy $E(x,g)$ (depending also on f and $\hat{\ell}$) as an appropriate average of $\varepsilon_i(x,f)$ and $\varepsilon_p(x,\hat{\ell}\circ g)$, where $\hat{\ell}\circ g\colon C \to [0,1]$ is defined as $\hat{\ell}\circ g(c) = \hat{\ell}(g(c))$, that is,

$$E(x,g) = w_i\ \varepsilon_i(x,f) + w_p\ \varepsilon_p(x,\hat{\ell}\circ g) \tag{1}$$

for some $w_i, w_p \in [0,1]$ with $w_i + w_p = 1$ or, more generally, as

$$E_q(x,g) = \|\langle w_i\ \varepsilon_i(x,f), w_p\ \varepsilon_p(x,\hat{\ell}\circ g)\rangle\|_q, \tag{2}$$

where $\|\cdot\|_q$ is a q-norm for $1 \le q \le \infty$. (More on the q-norms in the next sections.) Notice that E given by (1) is equal to E_1, that is, it is obtained by the use of 1-norm.

For a pair $\langle x, g\rangle$ minimizing E_q, we will consider x as the desired delineation and a transformation g as the mapping corresponding to optimal recognition. Note that by changing the weight values assigned to w_i and w_p we can modify the energy function in terms of the importance given to recognition versus delineation. In particular, if the global recognition method is able to bring the model (prior) sufficiently close to the actual object in I, then by setting w_p to 0 we can modify $E_q(x,g)$ to perform essentially optimal delineation.

In a more restrictive sense, the energy E_2 has been already considered in [2] for a joint segmentation/registration optimization task. More precisely, it was used in [2] for the continuous images (i.e., with C being an open region Ω in $\mathbb{R}^3$) and the hard segmentations $x\colon C \to \{0,1\}$. Both energies, ε_i and ε_p, were equal to the square root of the active contour model energy from [1]. The prior was simply an image of the same object with a given segmentation $\ell\colon C \to \{0,1\}$. (Notice, however, that the active contour model energy component ε_p uses the intensity f of the segmented image, unlike the model given by (2).)

We are not aware of similar optimization results formulated explicitly for the digital images on recognition and delineation and with adjustable emphasis, the subject of the next section.

2. q-NORM BASED ENERGY FOR DIGITAL IMAGES

From now on, we assume that the images are digital, defined on a finite scene C with a given adjacency relation. Fix a $q \in [1, \infty)$ (with an emphasis on $q = 2$ and $q = 1$).

- To each pair $\{c, d\}$ of adjacent spels in C we associate its *affinity* value $w_{c,d}$. An example is a simple version of a homogeneity based affinity: $w_{c,d} = \exp(-\|f(c) - f(d)\|)$. (Note that this depends on f.) But other affinities (or cost functions), like scale-based or even model-based, can also be used.
- To each fuzzy segmentation x we associate a vector/functional $F_i(x, f) = \langle w_{c,d}|x(c) - x(d)|\rangle_{c,d \text{ adjacent}}$. Note that, for the case of hard segmentations x, $|x(c) - x(d)|$ is 1 for an object boundary edge $\langle c, d\rangle$ and 0 otherwise.
- Define $\varepsilon_i(x, f)$ via formula $\|F_i(x, f)\|_q = \left(\sum_{c,d \text{ adjacent}} (w_{c,d}|x(c) - x(d)|)^q\right)^{1/q}$ or, equivalently, as its qth power: $(\|F_i(x, f)\|_q)^q = \sum_{c,d \text{ adjacent}} (w_{c,d}|x(c) - x(d)|)^q$. For $q = 1$ this is the standard GC energy; for $q = 2$ — the Random Walk, RW, energy.
- Notice that (as we proved recently [6]) the RFC energy is just the ∞-norm energy: $\varepsilon_i(x, f) = \|F_i(x, f)\|_\infty = \max_{c,d \text{ adjacent}} w_{c,d}|x(c) - x(d)|$.

Similarly, for a prior $L = \hat{\ell} \circ g \colon C \to [0, 1]$ and a vector/functional $F_p(x, L) = \langle |x(c) - L(c)|\rangle_{c \in C}$, the q-norm based energy $\varepsilon_p(x, \vec{p})$ is defined as

$$\varepsilon_p(x, L) = \|F_p(x, L)\|_q = \sqrt[q]{\sum_{c \in C} |x(c) - L(c)|^q}.$$

Thus, $\varepsilon_p(x, \hat{\ell} \circ g) = \|F_p(x, \hat{\ell} \circ g)\|_q = \sqrt[q]{\sum_{c \in C} |x(c) - \hat{\ell}(g(c))|^q}$. Once again, the ∞-norm energy version for $\varepsilon_p(x, L)$ is defined as

$$\varepsilon_p(x, L) = \|F_p(x, L)\|_\infty = \max_{c \in C} |x(c) - L(c)|,$$

that is, $\varepsilon_p(x, \hat{\ell} \circ g) = \|F_p(x, \hat{\ell} \circ g)\|_\infty = \max_{c \in C} |x(c) - \hat{\ell}(g(c))|$.

In summary, for $1 \le q < \infty$, we get

$$E_q(x, g) = \sqrt[q]{[w_i\ \varepsilon_i(x, f)]^q + [w_p\ \varepsilon_p(x, \hat{\ell} \circ g)]^q} = \sqrt[q]{\sum_{c,d \text{ adjacent}} [w_i\ w_{c,d}|x(c) - x(d)|]^q + \sum_{c \in C} [w_p\ |x(c) - \hat{\ell}(g(c))|]^q}$$

and, for $q = \infty$,

$$E_\infty(x, g) \quad = \quad \max \left\{ \max_{c,d \text{ adjacent}} [w_i\ w_{c,d}|x(c) - x(d)|], \max_{c \in C} [w_p\ |x(c) - \hat{\ell}(g(c))|] \right\}. \tag{3}$$

In what follows, we will restrict our attention to the group $\mathcal{G}$ of affine transformations of $\mathbb{R}^3$. Since in such case any $g \in G$ is identified by a 12 parameter vector $\vec{p} \in \mathbb{R}^{12}$ (referred to as *pose*), we will often write $E_q(x, \vec{p})$ for $E_q(x, g)$.

2.1. Cases of $q = 1, 2, \infty$

For $q = 1$, the energy E_q becomes

$$E_1(x, g) \quad = \quad \sum_{c,d \text{ adjacent}} w_i\ w_{c,d}|x(c) - x(d)| + \sum_{c \in C} w_p\ |x(c) - \hat{\ell}(g(c))|.$$

This is the Graph Cut, GC, type of energy. In fact, with $\hat{\ell}(g(c))$ replaced by a (not clearly defined) number x_c, this energy was suggested in [3]. However, it was not discussed there in such generality, as the authors discussed E_1 only with $x_i = 1$ and $x_p = 0$.

For $q = 2$, the square of the energy becomes

$$(E_2(x,g))^2 \quad = \quad \sum_{c,d \text{ adjacent}} [w_i \; w_{c,d}|x(c) - x(d)|]^2 + \sum_{c \in C} [w_p \; |x(c) - \hat{\ell}(g(c))|]^2.$$

This is the Random Walk, RW, type of energy [4]. Once again, in such a form (with $\hat{\ell}(g(c))$ replaced by x_c) it appears in [3], but was considered only with $w_i = 1$ and $w_p = 0$.

For $q = \infty$, the energy is given by (3) and it becomes a Relative Fuzzy Connectedness, RFC, type of energy, as shown in [6].

3. ALGORITHMS FOR FINDING MINIMIZERS OF E_q

We will present here a general iterative procedure that finds a pair $\langle x, \vec{p} \rangle$ that (approximately) minimizes $E_q(x, \vec{p})$. We will set up the problem for fuzzy segmentations x, which can be turned to hard segmentations by simple thresholding: the object is defined as $\{c \in C \colon x(c) > 0.5\}$. The problem of finding optimized hard segmentations will be discussed for each case of $q = 1, 2, \infty$ separately.

E_q is a function of two (general) variables: x and $\vec{p}$. Assuming that we have a way of minimizing it in each variable separately, we follow the following simple iterative procedure.

1. Start with an initial pose $\vec{p}_0$; it can be found by some optimization such as the global methods of recognition mentioned earlier;
2. Find $x_0 = x_{\vec{p}_0}$ minimizing $E_q(\cdot, \vec{p}_0)$;
3. Find $\vec{p}_1 = \vec{p}_{x_0}$ minimizing $E_q(x_0, \cdot)$;
4. Find $x_1 = x_{\vec{p}_1}$ minimizing $E_q(\cdot, \vec{p}_1)$;
5. Repeat steps 3 and 4 to find $\vec{p}_{n+1}$ and x_{n+1} from $\vec{p}_n$ and x_n until the number $E_q(x_n, \vec{p}_n) - E_q(x_{n+1}, \vec{p}_{n+1})$ does not go below some threshold θ;
6. Return the last values $\vec{p}_{n+1}$ and x_{n+1}.

Note that the algorithm always stops, at which time $E_q(p_{n+1}, x_{n+1})$ approximates a local minimum of E_q.

In what follows we discuss how to find, for a fixed pose $\vec{p}$, a global minimizer of $E_q(\cdot, \vec{p})$ for $q = 1, 2, \infty$. However, the minimizer returned by the above algorithm need not be optimal. Its optimality depends on the choice of the initial pose $\vec{p}_0$.

In the rest of this section we assume that a pose $\vec{p}$ is fixed, $g \in \mathcal{G}$ is associated with $\vec{p}$, and that $x_c = \hat{\ell}(g(c))$ for every $c \in C$.

3.1. Case $q = 2$: Random Walk

We need to find a minimizer of

$$\varepsilon_2(x) = \sum_{c,d \text{ adjacent}} [w_i \; w_{c,d}|x(c) - x(d)|]^2 + \sum_{c \in C} [w_p(x(c) - x_c)]^2.$$

Since $\varepsilon_2(x)$ is strictly convex, it has a uniquely defined minimizer. Moreover, it is achieved when all partial derivative of ε_2 are zero, that is, when $\nabla_x \varepsilon_2(x) = 0$. Since $\nabla_x \varepsilon_2(x) = 0$ constitutes a sparse system of linear equations, it can be solved by standard linear programing methods.

Notice, however, that the resulting minimizer is fuzzy. The problem of optimizing $\varepsilon_2(x)$ over the hard segmentations $x \colon C \to \{0, 1\}$ seems to be intractable.

3.2. Case $q = 1$: Graph Cut

We need to find a minimizer of $\varepsilon_1(x) = \sum_{c,d \text{ adjacent}} w_i \; w_{c,d}|x(c) - x(d)| + \sum_{c \in C} w_p|x(c) - x_c|$. We consider here only the case when $w_p > 0$, since in the case of $w_p = 0$ the information from the prior, the key component of this discussion, is not used. Then, $\varepsilon_1(x) = w_p \left[\sum_{c,d \text{ adjacent}} \frac{w_i \; w_{c,d}}{w_p}|x(c) - x(d)| + \sum_{c \in C} |x(c) - x_c|\right]$. In particular, the minimization of ε_1 is equivalent to the minimization of the energy

$$\hat{\varepsilon}_1(x) = \sum_{c,d \text{ adjacent}} \hat{w}_{c,d}|x(c) - x(d)| + \sum_{c \in C} |x(c) - x_c|,$$

where $\hat{w}_{c,d} = \frac{w_i \; w_{c,d}}{w_p}$. The energy $\hat{\varepsilon}_1$ is optimized over the hard segmentations $x \colon C \to \{0, 1\}$. For this, we will use the standard GC min cut/max flow algorithm, say as in [7], with the graph on $C \cup \{s, t\}$ (s being a source, t a sink) having the weights $\hat{w}_{c,d}$ as above and the source and sink weights are defined via

($\star$) $\hat{w}_{t,c} = 1 - x_c$ and $\hat{w}_{s,c} = x_c$ for every $c \in C$.

It is easy to see the hard segmentation associated with the min cut minimizing the graph with such weight assignments indeed minimizes the energy ε_1 (over the hard segmentations). This is so, since the graph cost function of the cut associated with $x \colon C \to \{0, 1\}$ is equal to $\hat{\varepsilon}_1(x)$.

3.3. Case $q = \infty$: (Iterative) Relative Fuzzy Connectedness

We should minimize the energy $\varepsilon_\infty(x) = \max\{\max_{c,d \text{ adjacent}}[w_i w_{c,d}|x(c) - x(d)|], \max_{c \in C}[w_p|x(c) - x_c|]\}$. However, for $w_p > 0$ it is not clear how to find the minimizer for such energy. More importantly, in such format the two energy components, $w_i\varepsilon_i(x)$ and $w_p\varepsilon_p(x)$, compete rather than synergistically strengthen each other. Therefore, for the "$q = \infty$" case we combine the ℓ_∞-norm internal energy $\varepsilon_i(x) = \max_{c,d \text{ adjacent}} w_{c,d}|x(c) - x(d)|$ with the ℓ_1-norm prior-based energy $\varepsilon_p = \sum_{c \in C} |x(c) - \hat{x}_c|$, where $\hat{x}_c = 0.5$ whenever $x_c \in (0, 1)$ and $\hat{x}_c = x_c$ otherwise. The minimized energy will have the form

$$\hat{\varepsilon}_\infty(x) = w_i \; \varepsilon_i(x) + w_p \; \varepsilon_p = \max_{c,d \text{ adjacent}} w_i \; w_{c,d}|x(c) - x(d)| + w_p \sum_{c \in C} |x(c) - \hat{x}_c|. \tag{4}$$

We consider the minimization of this energy only over the hard segmentations $x \colon C \to \{0, 1\}$. In addition, we assume that $w_p < 1$ is "considerably" larger than $w_i > 0$. (For the argument below it is enough to assume that $2w_i \; \max_{c,d \text{ adjacent}} w_{c,d} < w_p$. Since, for the standard weight choice we have $\max_{c,d \text{ adjacent}} w_{c,d} \leq 1$, this leads to the inequality $2w_i < w_p$. In such a case, any $w_p \in (2/3, 1)$ will be good enough.)

Notice, that under such assumptions, any hard segmentation $x \colon C \to \{0, 1\}$ minimizing $\hat{\varepsilon}_\infty$ must have the property that

($*$) $x(c) = \hat{x}_c$ whenever $\hat{x}_c \in \{0, 1\}$, that is, the object indicated by x contains $S = \{c \in C \colon \hat{x}_c = 1\}$ and is disjoint with $T = \{c \in C \colon \hat{x}_c = 0\}$.

Therefore, if we treat S and T as the sets of seeds indicating the foreground and the background, respectively, then any minimizer of $\hat{\varepsilon}_\infty$ agrees with such seeds indication. In particular, it is enough to search for the minimizer of $\hat{\varepsilon}_\infty$ within the family $\mathcal{P}(S, T)$ of all hard segmentations $x \colon C \to \{0, 1\}$ satisfying ($*$).

Next, notice that for any x from $\mathcal{P}(S, T)$, the value of $\varepsilon_p(x) = \sum_{c \in C} |x(c) - \hat{x}_c|$ is constant, equal to half of the size of the set $C \setminus (S \cup T) = \{c \in C \colon \hat{x}_c = 0.5\}$. Thus, the minimization of $\hat{\varepsilon}_\infty$ over $\mathcal{P}(S, T)$ is the same as the minimization of the energy $\varepsilon_i(x) = \max_{c,d \text{ adjacent}} w_{c,d}|x(c) - x(d)|$ over $\mathcal{P}(S, T)$.

Finally, notice that the energy $\varepsilon_i(x) = \max_{c,d \text{ adjacent}} w_{c,d}|x(c) - x(d)|$ is identical to the energy $\varepsilon^{\max}$ considered in [6], where it is proved that its minimizer over $\mathcal{P}(S, T)$ is the Iterative Relative Fuzzy Connectedness, IRFC, object which is returned, in linear time, by the algorithm $\text{GC}_{\max}$, a version of the Optimal Spanning Forest algorithm. This fact is the key theoretical motivation behind the experiments presented in the next section.

4. EXPERIMENTAL RESULTS

This section describes some preliminary results on the optimizations as described above. In particular, the algorithms used in the experiments utilized a non-iterative version involving only the first two steps described

in Section 3, rather than the full iterative schema. Moreover, in the experiments we used only the energy function $\hat{\varepsilon}_\infty$, defined via formula (4), where the parameters $\hat{x}_c$ are slightly modified, as described below. The full experimental justification of the different methods presented above is still a work in progress.

The algorithm uses the following general steps, where I is an image:

1. The pose $\vec{p}_0$ is found according to the recognition optimization method described in [8], as follows. The recognition method follows the hierarchical approach described in [8, 9] wherein different methods are presented which differ in only the optimality criterion that is used. For the experiments in this paper, we used the threshold-based optimality strategy wherein the object to be recognized and delineated is characterized by a threshold interval J. In this strategy, p_0 corresponds to the pose at which the volume of the regions corresponding to an exclusive or operation between the thresholded I (for threshold interval J) and the thresholded prior (for a membership value > 0.5) is minimized.

   Let $L = \hat{\ell} \circ g \colon C \to [0,1]$ be a prior associated with the pose $\vec{p}_0$.

2. Find the IRFC segmentation of the image I via algorithm $\mathrm{GC}_{\max}$ used with the object-indicating set S of seeds defined as

$$S = \{c \in C \colon \hat{\ell}(g(c)) > 0.5 \ \&\ f(c) \in J\}, \quad J \text{ being some interval of typical intensities for the object}$$

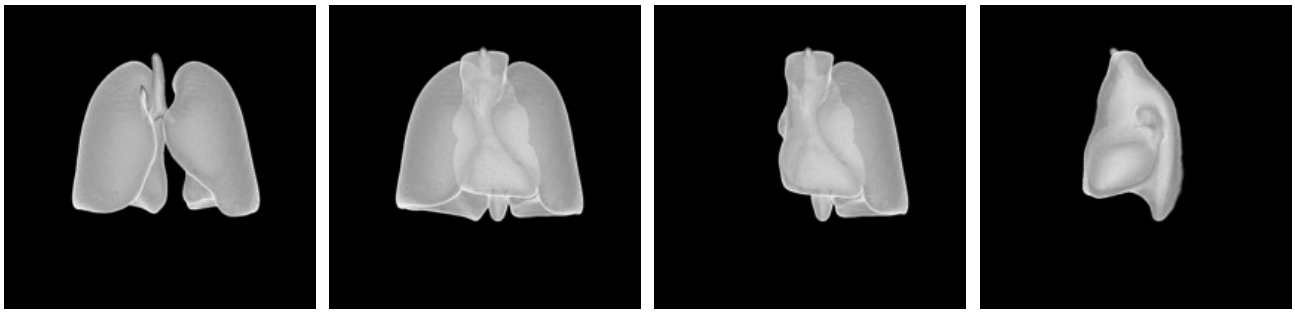

Figure 1. Volume renditions of different combinations of fuzzy models of objects: RS, RS & IMS, LPS & IMS, IMS.

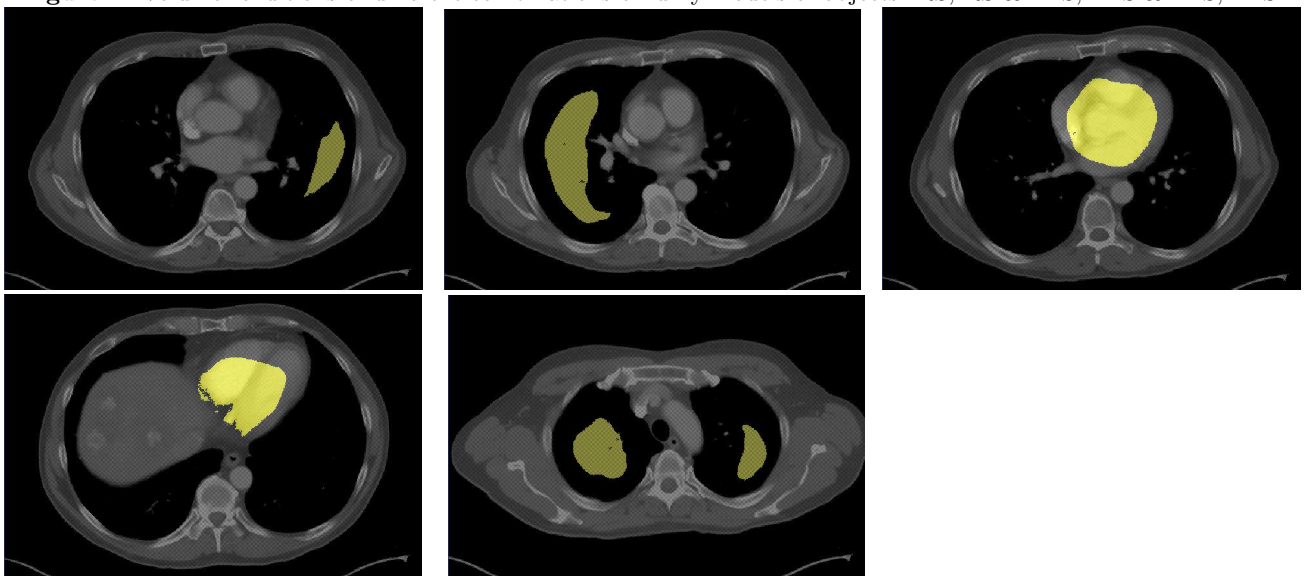

Figure 2. Seed sets automatically found for LPS, RPS, PC, IMS, and RS, respectively, overlaid on sample slices of test images. The seed appear as uniform gray (green, in color) region inside the respective objects.

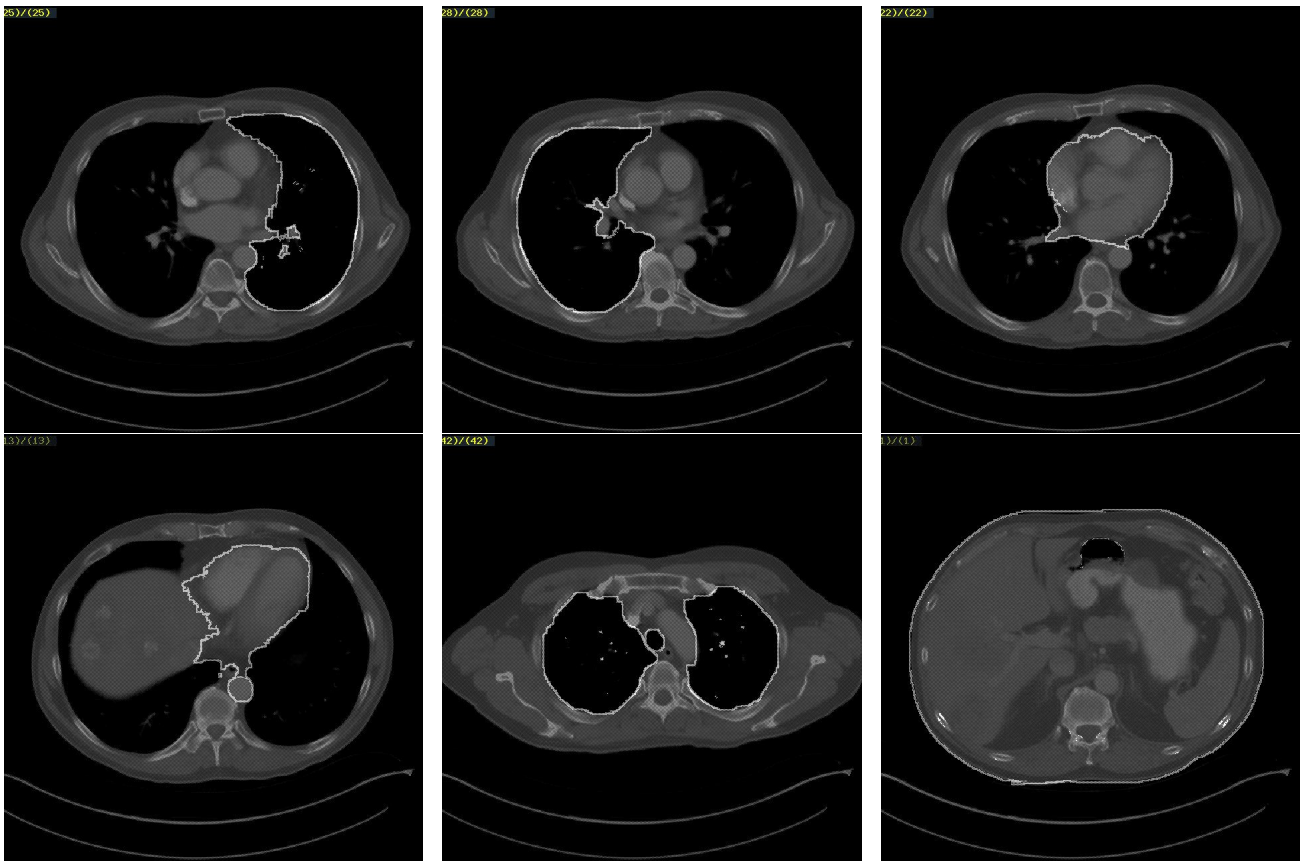

Figure 3. Delineation results for LPS, RPS, PC, IMS, RS, and Skin, respectively. Outlines of objects are shown overlaid on sample slices.

and the background-indicating set T of seeds defined as $T = \{c \in L(c) = 0\}$. Notice that, as argued in Section 3.3, the resulting IRFC object minimizes the energy $\hat{\varepsilon}_\infty$, where the numbers $\hat{x}_c$ are defined for each $c \in C$ as

$$\hat{x}_c = \begin{cases} 1 & \text{for } c \in S \\ 0 & \text{for } c \in T \\ 0.5 & \text{otherwise.} \end{cases}$$

The IRFC algorithm $\mathrm{GC}_{\max}$, as any pI-based fuzzy connectedness method, is based on the affinity $\mu(c, d)$ function which consists of the traditional homogeneity-based (ψ) and image intensity-based (φ) components. Additionally, a third component (ρ) based on the model is incorporated into μ to bring spatial constraints derived from the model (prior) L into connectedness. That is, $\mu(c, d) = \psi(c, d)+\varphi(c, d)+\rho(c, d)$. The model component is taken to be $\rho(c, d) = x_c$. Since the weight function is an inverse of affinity, an appropriate inverse of $\mu(c, d)$ is taken to be $w_{c,d}$.

We use the data sets and the set up of the AAR methodology we developed in [8, 9] for conducting our experiments. In this paper, we used the 40 CT data sets of the thoracic body region; 20 data sets were used for model building and the rest for testing.

Figure 1 shows volume renditions of the fuzzy models of some of the objects considered in this body region. Figure 2 displays object seed sets determined automatically by the global recognition strategy. The seed sets are overlaid on the slice display of the test images for different objects. Figure 3 presents delineation results as

boundary outlines overlaid on the slice display of test images. Table 1 lists the False Positive and True Positive volume fractions for the different objects. Average values over the 20 data sets are shown. Object abbreviations are as follows: RS—Respiratory System which we define as a union of trachea, bronchi, left pleural space (LPS), and right pleural space (RPS); IMS—Internal Mediastinum defined as a union of pericardium, arterial system, venous system, and esophagus; PC—Pericardium.

	IMS	**LPS**	**PC**	**RPS**	**RS**	**Skin**
FPVF	**0.02**	**0.001**	**0.01**	**0.001**	**0.002**	**0.004**
TPVF	**0.87**	**0.95**	**0.89**	**0.94**	**0.95**	**0.97**

Table 1. Average False Positive Volume Fraction (FPVF) and True Positive Volume Fraction (TPVF) for the delineation method.

5. CONCLUDING REMARKS

In this paper we demonstrated some preliminary results for the delineation part of our AAR methodology. After gaining some practical experience with different body regions, we are beginning to realize the virtue of breaking up the AAR segmentation task into *recognition* and *delineation*. It is of paramount importance to get the global recognition step to perform well—in the sense of setting all initialization conditions for delineation correctly—for the delineation method to perform well. This means that, without fail, the seeds should be 100% correctly indicated implying that the object seeds should be properly inside the object region and background seeds should be properly outside. Otherwise all seed-based delineation algorithms will perform wrongly. At present we do not have enough insight into how much the refined recognition process in the iterative optimization steps really buys in improving performance or even in steering away the solution from the above accurate condition of seed specification. Some early experiments along the lines presented in the previous section with GC algorithms have not yielded satisfactory results exactly because of their sensitivity to seed set size and location (unlike IRFC). Thus the property of robustness of the delineation algorithm to seeds seems to play an influential role in effective recognition, a concept which we have previously not realized. In other words, the FC algorithms seem to have an advantage in working effectively in tandem with recognition algorithms because their results are not sensitive to seed location inside the object and since they do not require large seed sets (unlike the shrinking problem of GC). The latter robustness property implies that it is much easier to specify a small seed set properly fully inside an object than to create a seed set sufficiently close to the real boundary to be delineated.

The above observations also imply that sparse objects, such as tubular structures, are a real challenge for effective recognition in the above sense. Our current efforts are focused on this issue and in further improving the hybrid delineation strategies presented in this paper.

Acknowledgement Udupa's work is supported by a DHHS grant HL105212.

REFERENCES

1. Chan, T., Vese, L.: "Active Contours Without Edges," *IEEE Trans. Image Process* 10(2), 266–277 (2001).
2. B. Vemuri, J. Ye, Y. Chen, C. Leonard: "Image registration via level-set motion: applications to atlas-based segmentation," *Med. Image Anal.* 7 (1) (2003) 1–20.
3. Camille Couprie, Leo Grady, Laurent Najman, and Hugues Talbot, "Power Watersheds: A Unifying Graph-Based Optimization Framework," *IEEE Trans. Pattern Anal. Machine Intell.* **33**(7) (2011), 1384–1399.
4. L. Grady: "Random walks for image segmentation," IEEE Transactions on PAMI, 28(11):1768–1783, 2006.
5. A.K. Sinop and L. Grady: "A seeded image segmentation frame – work unifying graph cuts and random walker which yields a new algorithm," *Proc. of ICCV'07*, 2007.
6. K.C. Ciesielski, J.K. Udupa, A.X. Falcão, P.A.V. Miranda, "Fuzzy Connectedness image segmentation in Graph Cut formulation: A linear-time algorithm and a comparative analysis," *Journal of Mathematical Imaging and Vision* **44**(3) (2012), 375–398.

7. Y. Boykov, O. Veksler, and R. Zabih, Fast approximate energy minimization via graph cuts. *IEEE Trans. Pattern Anal. Machine Intell.* **23**(11) (2001), 1222–1239.
8. J.K. Udupa, D. Odhner, A.X. Falcao, K.C. Ciesielski, P.A.V. Miranda, M. Matsumoto, G.J. Grevera, B. Saboury, and D.A. Torigian, Automatic anatomy recognition via fuzzy object models, *Medical Imaging 2012: Image Processing,* SPIE Proceedings 8316, 2012.
9. Jayaram K. Udupa, Dewey Odhner, Monica Matsumoto, Yubing Tong, Krzysztof C. Ciesielski, Pavithra Vaideeswaran, Victoria Ciesielski, Babak Saboury, Liming Zhao, Seyedmehrdad Mohammadianrasanani, Drew A. Torigian, Fuzzy-Model-Based Body-wide Anatomy Recognition in Medical Images, *Medical Imaging 2013*, SPIE Proceedings, paper # 8671-83.
10. Torsten Rohlfing, Robert Brandt, Randolf Menzel, Daniel Russakoff, and Calvin Maurer: "*Quo Vadis*, Atlas-Based Segmentation?," HANDBOOK OF BIOMEDICAL IMAGE ANALYSIS, Topics in Biomedical Engineering, 2005, pp. 435–486.